ferent cases of doubling the unit-cell volume, for instance doubling in the **c** direction or in the *c* plane as exemplified above.

Also, in their Table 5 a minimum volume ratio of eight is assigned to the subgroups D_{4h}^5, D_{4h}^7, D_{4h}^9, D_{4h}^{10} and of four to the subgroup D_{4h}^{11} of the space group D_{4h}^1 whilst according to the example above this volume ratio is two. (No other errors have been found however.)

May hearty thanks are due to Dr Forrest L. Carter, guest scientist from the Naval Research Laboratory, Washington, D. C., for improvements in style and presentation.

References

BÄRNIGHAUSEN, H. (1975). *Acta Cryst.* A**31**, S3.
BELOV, N. V., NERONOVA, N. N. & SMIRNOVA, T. S. (1957). *Kristallografiya*, **2**, 315–340.
BERTAUT, E. F. (1975*a*). *Ann. Phys.* (*F*), **9**, 93–108.
BERTAUT, E. F. (1975*b*). *Ann. Phys.* (*F*), **9**, 109–124.
BERTAUT, E. F. (1976). *Acta Cryst.* A**32**, 380–387.
BOYLE, L. L. & LAWRENSON, J. E. (1972). *Acta Cryst.* A**28**, 489.
HERMANN, C. (1929). *Z. Kristallogr.* **69**, 533.
Internationale Tabellen zur Bestimmung von Kristallstrukturen (1935). Vol. I. Berlin: Borntraeger.
International Tables for X-ray Crystallography (1952). Vol. I. Birmingham: Kynoch Press.
MARINDER, B. O. (1963). *Ark. Kem.* **19**, 435.
NEUBÜSER, J. & WONDRATSCHEK, H. (1966). *Krist. Tech.* **1**, 529–543.
OPECHOWSKI, W. & GUCCIONE, R. (1965). *Magnetism*, Vol. IIA, edited by G. T. RADO & H. SUHL, pp. 105–165. New York: Academic Press.
SHAPIRO, S. M., AXE, J. D., SHIRANE, G. & RACCAH, P. M. (1974). *Solid State Commun.* **15**, 377–381.
WONDRATSCHEK, H. & NEUBÜSER, J. (1970). Aachen Meeting, IUCr Commission on International Tables (unpublished).

Acta Cryst. (1976). A**32**, 983

Neutron Small-Angle Scattering by Dislocations in Homogeneously Oriented Nematic Liquid Crystals

BY ALFREDO OLIVEI

Advanced Technology Center, Olivetti S.p.A., 10015-*Ivrea, Italy*

(*Received* 2 *April* 1976; *accepted* 16 *May* 1976)

A complete examination of the shape of the neutron-scattering cross-section curves at very small scattering vectors, of the order of $0{\cdot}05 \sim 0{\cdot}1$ nm^{-1}, has been made for homogeneously oriented nematic liquid crystals. It is shown that the shape of the scattering curves at small angles is mainly determined by the kind of dislocation configuration exhibited by homogeneously oriented nematic liquid crystals. This study will furnish a partial guide to the construction of scattering relations for any kind of possible dislocation configuration in homogeneously oriented nematic liquid crystals, *e.g.* for stationary straight edge dislocations, moving edge dislocations, oscillating edge dislocations, curved dislocations and dislocation networks.

1. Small-angle scattering of neutrons and X-rays by dislocations in homogeneously oriented nematic liquid crystals

In a previous paper (Olivei, 1973) we have already discussed the usefulness of using cold-neutron scattering for probing the molecular structure of homogeneously oriented nematic liquid crystals in the absence of any external magnetic or electric fields. In that paper, however, we did not examine the cold-neutron scattering at very small values of the scattering vector (of the order of $0{\cdot}05 \sim 0{\cdot}1$ nm^{-1}). In fact, such a study should yield very interesting results about the existence and the structure of dislocations in homogeneously oriented nematic liquid-crystal layers.

The existence of lines or regions of discontinuity in the ordered structure of homogeneously oriented nematic liquid-crystal layers makes possible the setting up of dislocations of various kinds.

The use of cold-neutron small-angle scattering for studying dislocations in homogeneously oriented nematic liquid-crystal structures has advantages as compared to X-ray scattering. In principle, small-angle scattering of X-rays and neutrons is induced by long-range fluctuations of density or refractive index in a sample. Such fluctuations are produced by many types of structural disorder, *e.g.* dislocations, defect clusters, critical phenomena.

The first advantage of neutrons as compared to X-rays concerns the change of the wavelength. In most

cases, X-ray experiments are performed in the range of 1·5 Å. With neutrons the liquid-crystal sample absorption is relatively low and wavelengths between 5 and 15 Å can be used easily. It is even possible to go to 20 Å or more.

The advantage of the greater wavelength is twofold: Bragg scattering is completely avoided, and therefore also double Bragg scattering, which induces an additional intensity at small angles masking the 'true' small-angle scattering.

The other advantage is due to the scattering law being for fundamental reasons a function of the scattering vector $\boldsymbol{\kappa}$ only, where (Olivei, 1973):

$$|\boldsymbol{\kappa}| = \frac{4\pi}{\lambda} \sin \theta/2 \tag{1}$$

(θ = scattering angle, λ = wavelength of the neutrons).

Under favourable conditions, the angular resolution is comparable for X-rays and neutrons. Therefore, the obtainable $|\boldsymbol{\kappa}|$ values can be a factor of ten smaller with neutrons than with X-rays. This means that fluctuations of relatively long range can be investigated in homogeneously oriented nematic liquid-crystal structures.

The main disadvantage of the neutron technique is the relatively low luminosity of neutron sources. This intensity disadvantage, however, can be compensated in experiments by using (i) very long instruments with large slit widths and (ii) focusing systems with totally reflecting mirrors to obtain large solid angles. Because we are only interested in the $|\boldsymbol{\kappa}|$ (and not in the θ) resolution, longer wavelengths can be applied which allow shorter instruments at comparable intensities.

Our presentation here of neutron small-angle scattering by dislocations in homogeneously oriented nematic liquid crystals will fall short of furnishing a complete guide to the construction of scattering relations, but will go a long way towards elucidating the physical–structural bases of such relations and hopefully will stimulate further detailed developments. We will find it useful now to start with a short account of the content of the present paper.

After a discussion of the essential features of the general formulae for neutron small-angle scattering from dislocations in homogeneously oriented nematic liquid crystals, the derivation of the scattering cross section for dislocations such as (i) stationary straight edge dislocations, (ii) moving edge dislocations and (iii) oscillating edge dislocations will allow the detection of the influence of diffusion processes and will provide at the same time a means for discriminating between stationary, moving and oscillating dislocations, simply by inspection of the experimental scattering curves and comparison of them with the theoretical ones.

A further step in the refinement of our theoretical tools is represented by the consideration of dislocation loops consisting of finite numbers of straight segments, which will strengthen the theoretical analysis by approaching more closely physical reality. The study of curved dislocations such as circular dislocation loops and helical dislocations will complete the analysis.

Finally the examination of dislocation networks, such as Frank dislocation networks (Owen & Mura, 1967), will provide a sound tool for inspecting and interpreting the most subtle experimental findings.

2. Essential features of the formulae for neutron small-angle scattering from dislocations

The scattering cross section for coherent disorder resulting from a given dislocational configuration can be obtained by immediate use of the Fourier transform of the fluctuations in density and displacement (Krivoglaz, 1969; Schmatz, 1975):

$$\frac{\mathrm{d}\sigma}{\mathrm{d}\Omega} = \frac{1}{N} a^2 |\tilde{\theta}|^2 \tag{2}$$

where

$$\tilde{\theta} = \frac{1}{\Omega_V} \int_V \frac{\varrho(\mathbf{r}) - \bar{\varrho}}{\bar{\varrho}} \exp i\boldsymbol{\kappa}\mathbf{r}\mathrm{d}\mathbf{r} = \frac{1}{\Omega_V} \int_V \operatorname{div} \mathbf{s} \exp i\boldsymbol{\kappa}\mathbf{r}\mathrm{d}\mathbf{r} \tag{3}$$

in the Fourier transform of the relative density difference or the divergence of the displacement field.

In the above expressions N is the number of atoms contained in the volume V of the sample probed by the incident neutron beam, a is the nuclear scattering length, $\Omega_V = V/N$ is the average atomic volume, $\bar{\varrho}$ is the mean density, $\varrho(\mathbf{r})$ is the density at position $\mathbf{r}$, $\boldsymbol{\kappa}$ is the scattering vector and $\mathbf{s}$ the displacement vector at position $\mathbf{r}$.

Homogeneously oriented nematic liquid-crystal structures are anisotropic from the elastic standpoint. This will cause the scattering to be more peaked in some directions than it would be for an elastically isotropic medium. Though the difference may be appreciable, conclusions so far drawn from small-angle scattering are little affected by the assumption of elastic isotropy. To this important question we will give more attention later, and in this section we will take for granted that the formulae used are very little affected by the assumption of elastic isotropy. The axis of anisotropy will, anyway, without exception always be taken in the z direction for the cases considered later.

For a given dislocation configuration, the expression of the divergence of the corresponding displacement field can be obtained essentially by two methods. The first one is the direct method, which consists of evaluating the components of the displacement field $\mathbf{s}$ and thence deducing the divergence of $\mathbf{s}$.

The second method uses the expression for the components of the stress field associated with the displacement field to obtain directly the divergence of the displacement field. By this method, if σ_x, σ_y and σ_z are the components of the stress field, ε_x, ε_y and ε_z are the components of the elongation strain and s_x, s_y and s_z the components of the displacement field, we have (Love, 1944)

$$\left.\begin{aligned}\varepsilon_x &= \frac{1}{\mu}[\sigma_x - \nu(\sigma_y+\sigma_z)] = \frac{\partial s_x}{\partial x}\\ \varepsilon_y &= \frac{1}{\mu}[\sigma_y - \nu(\sigma_x+\sigma_z)] = \frac{\partial s_y}{\partial y}\\ \varepsilon_z &= \frac{1}{\mu}[\sigma_z - \nu(\sigma_x+\sigma_y)] = \frac{\partial s_z}{\partial z}\end{aligned}\right\} \tag{4}$$

and

$$\operatorname{div}\mathbf{s} = \frac{\partial s_x}{\partial x} + \frac{\partial s_y}{\partial y} + \frac{\partial s_z}{\partial z} = \varepsilon_x + \varepsilon_y + \varepsilon_z\,, \tag{5}$$

μ and ν being the shear modulus and Poisson's ratio, respectively.

This method is usually straightforward and simpler than the direct method, in view also of the fact that the expressions for the stress field can be found in the literature for a large variety of cases and configurations of dislocations.

After the calculation of div **s**, it is necessary to evaluate numerically the integral (4) and to substitute the results in expression (2), which finally yields the numerical values of the small-angle scattering cross section.

As an application of the above formulae it is interesting to show that there is no contribution to scattering from pure screw dislocations. The components of the displacement field of a stationary straight screw dislocation along the z axis with a Burgers vector of magnitude b are (Burgers, 1939)

$$\left.\begin{aligned}s_x &= 0\\ s_y &= 0\\ s_z &= \frac{b}{2\pi}\tan^{-1}\frac{y}{x}\end{aligned}\right\} \tag{6}$$

and therefore

$$\operatorname{div}\mathbf{s} = 0 \tag{7}$$

which yields no scattering according to equation (3).

The same conclusion also holds for a straight screw dislocation parallel to the z axis and moving along the x axis with a uniform velocity v. In this case the components of the displacement field are given by (Frank, 1949)

$$\left.\begin{aligned}s_x(t) &= 0\\ s_y(t) &= 0\\ s_z(t) &= \frac{b}{2\pi}\tan^{-1}\frac{y(1-v^2/\beta^2)^{1/2}}{x-vt}\end{aligned}\right\} \tag{8}$$

with

$$\beta^2 = \mu/\varrho\,.$$

As a consequence

$$\operatorname{div}\mathbf{s}(t) = 0\,. \tag{9}$$

Even if we consider the more complex case of a straight screw dislocation oscillating in the neighborhood of the origin of coordinates with a small amplitude A and frequency ω, the result is always a zero contribution to scattering. In this case the total displacement is the sum of the stationary displacement given by (6) and the time-dependent displacement due to oscillations. The time-dependent part of the displacement field is given by (Eshelby, 1949*b*)

$$\begin{aligned}s_x(\omega,t) &= 0\\ s_y(\omega,t) &= 0\\ s_z(\omega,t) &= -\frac{bA\omega y}{4\beta R}[J_1(\omega R/\beta)\cos\omega t\\ &\quad + Y_1(\omega R/\beta)\sin\omega t]\\ &\quad + \frac{A\omega x}{\beta R}[J_2(2\omega R/\beta)\sin 2\omega t\\ &\quad - Y_2(2\omega R/\beta)\cos 2\omega t]\,,\end{aligned} \tag{10}$$

where $R=(x^2+y^2)^{1/2}$ and J and Y are Bessel functions of the first and the second kinds. The corresponding divergence of the total displacement field is again zero.

As a result of these simple examples, in the next sections we will mainly focus our attention on the study of edge-dislocation configurations which are strong sources of scattering, and we will consider only complicated configurations for screw dislocations, such as helical dislocations, which can yield some contribution to scattering.

3. Scattering cross section of a straight edge dislocation

3.1 *On the choice of the simplifying assumptions*

Now we are faced with two main problems in developing explicit expressions for the small-angle scattering cross section of a straight dislocation line: (1) the elastic anisotropy of the medium; (2) the finite length of the dislocation line. It has been already pointed out that the elastic anisotropy of the medium under consideration causes the scattering to be more peaked in some directions, for example in the direction perpendicular to the glide plane for an edge dislocation. Eshelby, Read & Shockley (1953) and Leibfried (1953) found the displacement and stress fields for an arbitrary homogeneous anisotropic solid when a straight dislocation along the z axis has an arbitrary Burgers vector. Since these solutions include constants which are roots of a sixth-order polynomial, explicit expressions are not possible except for a few special cases. Though the difference may be appreciable, conclusions that can be so far drawn from small-angle scattering are little affected by this assumption of elastic isotropy. Therefore we will take for granted the assumption of elastic isotropy in the calculations of the displacement and stress fields of any kind of dislocation.

With reference to the second point it is worth pointing out that the analytical expression for the displacement and stress fields depends on the length of the dislocation segment and, as a consequence, a corresponding dependence should be also expected for the analytical expression of the small-angle scattering cross section.

The sample of nematic liquid crystal under consideration has a finite thickness and therefore a straight dislocation line has a finite length determined by the spacing between boundary surfaces, which, however, are not free boundary surfaces. Therefore no additional term should be added to the expression for the stress field contributed from a straight dislocation segment, since the requirement that the total stress gives zero surface traction on the free boundary surface does not apply in this case.

The analytical expression for the displacement and stress fields contributed from a straight dislocation segment whose true length equals the thickness of the liquid-crystal layer is much more complicated than the corresponding expression from a straight dislocation of infinite or seminfinite length.

It is however extremely important to compare the theoretical shapes of the scattering cross sections for single straight dislocations having infinite, semi-infinite and finite lengths in order to evaluate the differences and the errors that are made by replacing expressions for single straight dislocations of finite length (equal to the spacing between parallel plates containing the nematic liquid crystal) with the much simpler expression for single straight dislocations of infinite length. These approximations would extremely facilitate the study of the small-angle scattering cross section of a single moving dislocation and a single oscillating dislocation.

We will show that differences exist in the shape of the dependence of the scattering cross section on the length assumed for the straight dislocation, but conclusions so far drawn from small-angle scattering for a moving dislocation and an oscillating dislocation by the assumption of infinite length are little affected.

It is immediately obvious that the use of such an approximations cannot be extended to the study of dislocation loops.

3.2 *Stationary straight edge dislocation*

Now let us consider first the more difficult case of a straight edge dislocation of finite length, l. The line of the dislocation is taken as the z axis, which is perpendicular to the parallel plates constraining the liquid crystal, Fig. 1.

The dislocation is stationary at the z axis. The direction of the Burgers vector is taken arbitrarily with components (b_x, b_y, b_z).

The components σ_x, σ_y and σ_z, of the stress dislocation field are

$$\sigma_x = \frac{\mu}{4\pi(1-\nu)}\left\{\frac{b_y x - b_x y}{x^2+y^2}\left(\frac{l-z}{\{x^2+y^2+(l-z)^2\}^{1/2}} + \frac{z}{\{x^2+y^2+z^2\}^{1/2}}\right) - \frac{xy(b_x x + b_y y)}{x^2+y^2}\left[\frac{l-x}{(x^2+y^2+z^2)^{1/2}} \times \left(\frac{1}{\{x^2+y^2+(l-z)^2\}^{1/2}} - \frac{2}{x^2+y^2}\right) - \frac{l-z}{(x^2+y^2+z^2)^{1/2}}\left(\frac{1}{(x^2+y^2+z^2)^{1/2}} - \frac{2}{x^2+y^2}\right)\right] + b_z xy\left(-\frac{1}{\{x^2+y^2+(l-z)^2\}^{3/2}} - \frac{1}{(x^2+y^2+z^2)^{3/2}}\right)\right\}, \tag{11}$$

$$\sigma_y = \frac{\mu}{4\pi(1-\nu)}\left\{\frac{b_y x - b_x y}{x^2+y^2}\left(\frac{l-z}{\{x^2+y^2+(l-z)^2\}^{1/2}} - \frac{z}{\{x^2+y^2+z^2\}^{1/2}}\right) + \frac{xy(b_x x + b_y y)}{x^2+y^2} \times \left[\frac{l-z}{\{x^2+y^2+z^2\}^{1/2}}\left(\frac{1}{\{x^2+y^2+(l-z)^2\}^{1/2}} + \frac{2}{x^2+y^2}\right) - \frac{l-z}{\{x^2+y^2+z^2\}^{1/2}} \times \left(\frac{1}{\{x^2+y^2+z^2\}^{1/2}} + \frac{2}{x^2+y^2}\right)\right] - b_z xy\left(-\frac{1}{\{x^2+y^2+(l-z)^2\}^{3/2}} + \frac{1}{\{x^2+y^2+z^2\}^{3/2}}\right)\right\}, \tag{12}$$

$$\sigma_z = \frac{\mu\nu}{2\pi(1-\nu)}\frac{b_y x - b_x y}{x^2+y^2} \times \left(\frac{l-z}{\{x^2+y^2+(l-z)^2\}^{1/2}} - \frac{z}{\{x^2+y^2+z^2\}^{1/2}}\right), \tag{13}$$

μ and ν being the shear modulus and Poisson's ratio respectively.

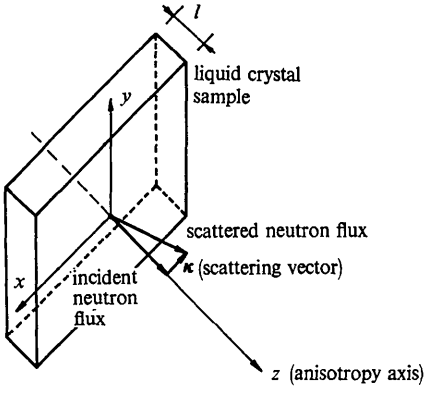

Fig. 1. General schematic configuration for neutron small-angle scattering, which will be adopted for all the cases without any exception.

Substitution of the three previous expressions into (4) yields the components of the strain field. Summing up the three strain components yields the divergence of the displacement field as shown by (5):

$$\begin{aligned}\operatorname{div}\mathbf{s}=\frac{1}{4\pi(1-\nu)}\Bigg\{&(1-\nu-\nu^3)\frac{b_yx-b_xy}{x^2+y^2}\\&\times\left(\frac{l-z}{\{x^2+y^2+(l-z)^2\}^{1/2}}+\frac{z}{\{x^2+y^2+z^2\}^{1/2}}\right)\\&-(1+\nu)\frac{xy(b_xx+b_yy)}{x^2+y^2}\left[\frac{l-z}{\{x^2+y^2+(l-z)^2\}^{1/2}}\right.\\&\times\left(\frac{1}{x^2+y^2+(l-z)^2}+\frac{2}{x^2+y^2}\right)\\&+\frac{z}{\{x^2+y^2+z^2\}^{1/2}}\\&\left.\times\left(\frac{1}{x^2+y^2+z^2}+\frac{2}{x^2+y^2}\right)\right]+(1+\nu)b_zxy\\&\times\left(\frac{1}{\{x^2+y^2+z^2\}^{3/2}}-\frac{1}{\{x^2+y^2+(l-z)^2\}^{3/2}}\right)\Bigg\}.\end{aligned}\tag{14}$$

The divergence of the displacement field contributed from a half-infinite dislocation is obtained simply from the limit $l\to\infty$ in equation (14):

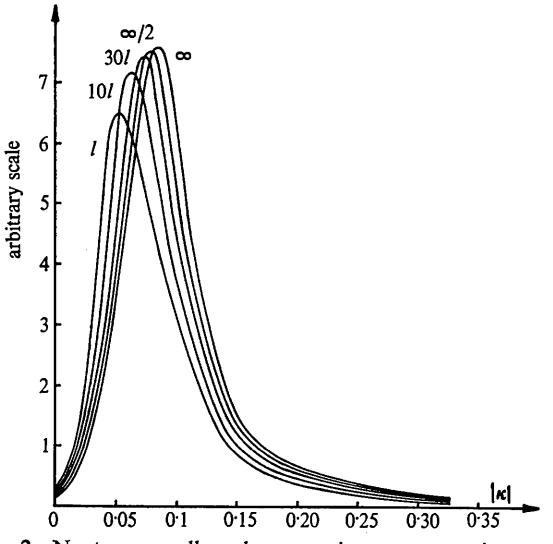

Fig. 2. Neutron small-angle scattering cross sections as a function of the scattering amplitude $|\kappa|$ for the significant case of κ perpendicular both to the slip direction (along the x axis) and the dislocation line (along the z axis) for a stationary edge dislocation having a true length l equal to the thickness of the liquid-crystal sample and for an edge dislocation having fictitious lengths which are multiples of l, notwithstanding that the true length of any dislocation under consideration remains unchanged and equal to l. The parameters of the MBBA homogeneously oriented nematic liquid crystal are: Poisson ratio $\nu=0{,}49$; shear modulus $\mu=10^{-5}$ Newton/m^2; $l=1$ μm; $b=0{,}05$ μm.

$$\begin{aligned}\operatorname{div}\mathbf{s}=\frac{1}{4\pi(1-\nu)}\Bigg\{&(1-\nu-\nu^3)\frac{b_yx-b_xy}{x^2+y^2}\\&\times\left(1+\frac{z}{\{x^2+y^2+z^2\}^{1/2}}\right)-(1+\nu)\frac{xy(b_xx+b_yy)}{x^2+y^2}\\&\times\left[\frac{2}{x^2+y^2}+\frac{z}{\{x^2+y^2+z^2\}^{1/2}}\right.\\&\left.\times\left(\frac{1}{x^2+y^2+z^2}+\frac{2}{x^2+y^2}\right)\right]\\&+(1+\nu)\frac{b_zxy}{\{x^2+y^2+z^2\}^{3/2}}.\end{aligned}\tag{15}$$

The displacement components of an edge dislocation of infinite length, with the line of dislocation taken as the z axis, are given by:

$$s_x(x,y,z)=\frac{b}{4\pi}\left(2\tan^{-1}\frac{y}{x}+\frac{1}{1-\nu}\frac{xy}{x^2+y^2}\right)\tag{16}$$

$$s_y(x,y,z)=\frac{b}{4\pi}\left(\frac{2\nu-1}{2(1-\nu)}\log(x^2+y^2)+\frac{1}{1-\nu}\frac{y^2}{x^2+y^2}\right)\tag{17}$$

$$s_z(x,y,z)=0\,,\tag{18}$$

where b is the magnitude of the slip, which occurs parallel to the x axis.

The divergence of the displacement field from an edge dislocation having a fictitious infinite length, the line of dislocation being taken as the z axis, is given by

$$\operatorname{div}\mathbf{s}=\frac{b}{2\pi}\frac{2\nu-1}{1-\nu}\frac{y}{x^2+y^2}.\tag{19}$$

The corresponding expression for the small-angle neutron scattering cross section for any of the previous cases is then obtained through the use of expressions (2) and (3).

The scattering cross section for a dislocation having a true length l in a nematic liquid-crystal layer having the same thickness is given by:

$$\frac{d\sigma}{d\Omega}=\frac{N}{V^2}a^2\left|\int_{-\infty}^{+\infty}dx\int_{-\infty}^{+\infty}dy\int_{-l}^{0}\operatorname{div}\mathbf{s}\,dz\right|^2.\tag{20}$$

The scattering cross sections for dislocations having a fictitious length larger than the true value l are obtained from (20) simply by taking the fictitious length as the lower limit of the far right-hand integral. For a dislocation having a fictitious infinite length the upper limit of the far right-hand integral in (20) becomes $+\infty$ and the lower limit $-\infty$.

The numerical integration of the previous multiple integral (20) yields the numerical values of the elastic small-angle scattering cross section $d\sigma/d\Omega$ for a cold-neutron beam of polarization p_0 incident on a stationary edge dislocation of finite, seminfinite or infinite length.

In Fig. 2 we have reported the shape of the small-angle scattering cross section $d\sigma/d\Omega$ as a function of

the amplitude of the scattering vector κ in the particular but very significant case of κ perpendicular both to the slip direction and to the dislocation line, the Burgers vector being situated along the x direction and the dislocation line along the z direction. It therefore results that the scattering vector κ is directed along the y axis.

A family of small-angle scattering cross-section curves is reported for an edge dislocation having a true length l equal to the thickness of the liquid-crystal layer and for edge dislocations having fictitious lengths which are a multiple of l, notwithstanding the fact that the true length of any dislocation under consideration remains unchanged and equal to l.

Inspection of Fig. 2 shows that the maximum of the intensity of the small-angle scattering cross-section curves increases for increasing values of the fictitious dislocation length, while the sample thickness remains unchanged.

The maxima are displaced slightly toward higher values of the scattering vector for increasing values of the sample thickness. The intensity at $|\kappa|=0$ decreases for increasing values of the thickness of the sample.

Slight differences exist between the theoretical scattering cross section resulting from a dislocation having a real length l, equal to the thickness of the nematic liquid-crystal layer, and those from dislocations of fictitious lengths which are multiples of the liquid-crystal layer thickness but remain unchanged when the dislocation length is fictitiously increased. Moreover, the theoretical differences arising from the assumption of infinite length instead of the true length for a straight dislocation affect very little the conclusions that can be drawn for interpreting the experimental results, notwithstanding that the liquid-crystal layer has a finite thickness l and the straight dislocation also has the same finite length.

As a consequence we will use the approximation of an infinite dislocation length for deriving the scattering cross sections resulting respectively from a moving and an oscillating straight dislocation in a nematic liquid-crystal sample of thickness l.

3.3 *Moving edge dislocation*

Let us consider a straight edge dislocation parallel to the z axis. The dislocation has a true length equal to the thickness, l, of the liquid-crystal layer. According to the results of the previous section, we will assume, however, a fictitious infinite length for the moving dislocation. This assumption will alter very slightly the final results and in return we will have to deal with simpler mathematical formulae.

The dislocation is moving along the x axis with a uniform velocity v. The position of the dislocation is denoted by $x=vt$ at time t. The components of the displacement field were first obtained by Eshelby (1949*a*). If at time t the slipped surface is defined by $y=0$ and $x<vt$ and the magnitude of the slip occurring in the x direction is denoted by b, then the components of the displacement field are given by

$$s_x=\frac{\beta^2 b}{\pi v^2}\left[\tan^{-1}\frac{y(1-v^2/\alpha^2)^{1/2}}{x-vt}+(v/2\beta^2-1)\tan^{-1}\frac{y(1-v^2/\beta^2)^{1/2}}{x-vt}\right], \tag{21}$$

$$s_y=\frac{\beta^2 b}{\pi v^2}\left\{(1-v^2/\alpha^2)^{1/2}\log\left[\frac{(x-vt)^2}{1-v^2/\alpha^2}+y^2\right]^{1/2}-\frac{1-v^2/2\beta^2}{(1-v^2/\beta^2)^{1/2}}\log\left[\frac{(x-vt)^2}{1-v^2/\beta^2}+y^2\right]^{1/2}\right\}, \tag{22}$$

$$s_z=0 \tag{23}$$

where

$$\alpha^2=(\lambda+2\mu)/\varrho\,, \tag{24}$$

$$\beta^2=\mu/\varrho\,, \tag{25}$$

$$\lambda=2\mu\nu/(1-2\nu)\,, \tag{26}$$

μ and ν being the shear modulus and Poisson's ratio respectively and ϱ the density of the material.

The explicit expression for the divergence of the displacement field can be obtained by differentiating expressions (21), (22), and (23) with respect to x, y and z respectively and summing up the results:

$$\operatorname{div}\mathbf{s}=\frac{\beta^2 b}{\pi v}\left\{(1-v^2/\alpha^2)^{1/2}\frac{2y-v^2/\alpha^2}{(x-vt)^2+y^2(1-v^2/\alpha^2)}-(1-v^2/2\beta^2)(1-v^2/\beta^2)^{1/2}\frac{2y}{(x-vt)^2+y^2(1-v^2/\alpha^2)}\right\}. \tag{27}$$

The elastic small-angle scattering cross section for a moving edge dislocation in a nematic liquid-crystal layer of thickness l in the approximation of a fictitious infinite length for the dislocation is given by:

$$\frac{\mathrm{d}\sigma}{\mathrm{d}\Omega}=\frac{N}{V^2}\alpha^2\frac{\beta^4 b^2}{\pi^2 v^2}\times\left|\int_{-\infty}^{+\infty}\mathrm{d}x\int_{-\infty}^{+\infty}\mathrm{d}y\int_{-\infty}^{+\infty}\left\{(1-v^2/\alpha^2)^{1/2}\times\frac{2y-v^2/\alpha^2}{(x-vt)^2+y^2(1-v^2/\alpha^2)}-(1-v^2/2\beta^2)(1-v^2/\beta^2)^{1/2}\times\frac{2y}{(x-vt)^2+y^2(1-v^2/\alpha^2)}\right\}\mathrm{d}z\right|^2. \tag{28}$$

The set of curves reported in Fig. 3 shows the changes undergone by the shape of the curve of the scattering cross section *versus* the scattering vector κ for increasing values of the uniform velocity of displacement of the dislocation. These curves have been traced for the particular but very significant case of κ perpendicular both to the slip direction and to the dislocation line, the Burgers vector being situated along the x direction and the dislocation line along the z direction.

With the scattering cross-section curve of a stationary dislocation as reference, the scattering cross-section

curves tend to flatten out and to become less and less sharp for increasing values of the displacement velocity of the dislocation. Therefore it should be easy to distinguish between stationary and moving dislocations by examining the shape of the experimental small-angle neutron-scattering cross-section curves.

In Fig. 4 we have drawn the equicontour lines $|\tilde{\theta}|^2$ for the relative scattered neutron intensity around an edge dislocation for several values of the uniform velocity of displacement in the x direction [the scattering vector κ is taken perpendicular both to the slip direction (x axis) and to the dislocation line (z axis)].

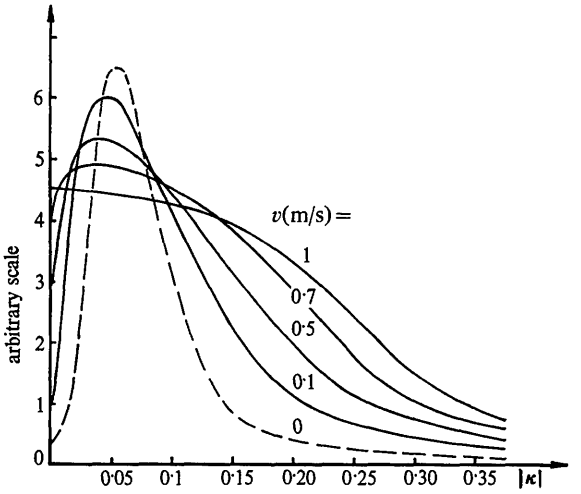

Fig. 3. Neutron small-angle scattering cross sections as a function of the scattering amplitude $|\kappa|$ [κ perpendicular both to the slip direction (x axis) and to the dislocation line (z direction)] for different values of the translation velocity of the edge dislocation in the x direction. For the parameters of the MBBA homogeneously oriented nematic liquid crystal see Fig. 2.

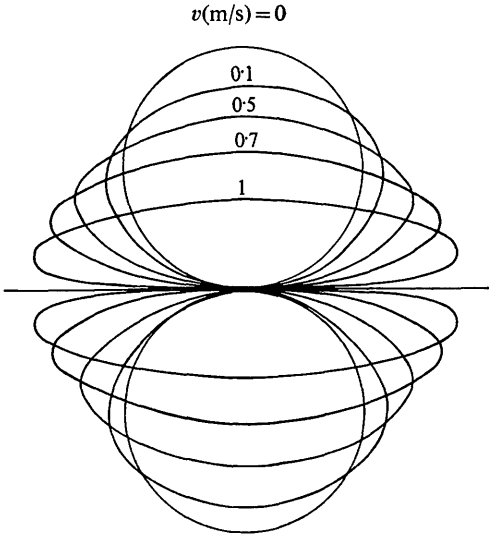

Fig. 4. Equicontour lines $|\tilde{\theta}|^2$ for the relative scattered neutron intensity around an edge dislocation for several values of the uniform velocity of dislpacement in the x direction [the scattering vector κ is taken perpendicular both to the slip direction (x axis) and to the dislocation line (z direction)]. For the parameters for the MBBA homogeneously oriented nematic liquid crystal see Fig. 2.

3.4 *Oscillating edge dislocation*

Consider a straight edge dislocation parallel to the z axis. The dislocation is oscillating in the neighborhood of the origin of coordinates with a small amplitude A.

The position of the dislocation is defined by:

$$x=A\sin\omega t\,,\quad y=0 \tag{29}$$

and the velocity by:

$$v(t)=A\omega\cos\omega t\,. \tag{30}$$

The displacement field $\mathbf{s}^*$ is the sum of the time-dependent field $\mathbf{s}_\omega(t)$ and the time-independent field $\mathbf{s}$. The components of the time-independent field, $\mathbf{s}$, are given by equations (16)–(18), while the time-dependent components of the displacement field were first obtained by Kiusalaas & Mura (1964). The components of the complete displacement field can be expressed in the form,

$$\begin{aligned} s_x^* &= s_x + s_{\omega x}(t)\\ s_y^* &= s_y + s_{\omega y}(t)\\ s_z^* &= 0\,. \end{aligned} \tag{31}$$

The terms s_x and s_y are the time-independent components of the displacement as given by equations (16)–(18), while $s_{\omega x}$ and $s_{\omega y}$ represent the time-dependent components of the displacement field and are given by:

$$\begin{aligned} s_{\omega x}(t) = -\frac{b_z K_\beta A}{8}\Big\{ & \Lambda^3\Big[Z_1^\alpha \sin\Big(\tan^{-1}\frac{x}{y}\Big) \\ & - Z_3^\alpha \sin 3\Big(\tan^{-1}\frac{y}{x}\Big)\Big] \\ & + Z_1^\beta \sin\Big(\tan^{-1}\frac{y}{x}\Big) + Z_3^\beta \sin 3\Big(\tan^{-1}\frac{y}{x}\Big)\Big\} \end{aligned} \tag{32}$$

$$\begin{aligned} s_{\omega y}(t) = -\frac{b_z K_\beta A}{8}\Big\{ & \Lambda^3\Big[Z_1^\alpha \cos\Big(\tan^{-1}\frac{y}{x}\Big) \\ & + Z_3^\alpha \cos 3\Big(\tan^{-1}\frac{y}{x}\Big)\Big] \\ & + Z_3^\beta \cos\Big(\tan^{-1}\frac{y}{x}\Big) - Z_3^\beta \cos 3\Big(\tan^{-1}\frac{y}{x}\Big)\Big\} \end{aligned} \tag{33}$$

$$s_{\omega z}(t)=0\,, \tag{34}$$

where

$$\begin{aligned} Z_n^\alpha &= Y_n(K_\alpha R)\sin\omega t + J_n(K_\alpha R)\cos\omega t\,,\\ Z_n^\beta &= Y_n(K_\beta R)\sin\omega t + J_n(K_\beta R)\cos\omega t\,,\\ R &= (x^2+y^2)^{1/2},\\ \Lambda &= K_\alpha/K_\beta\,,\quad K_\alpha=\omega/\alpha\,,\quad K_\beta=\omega/\beta\,,\\ \alpha^2 &= (\lambda+2\mu)/\varrho\,,\quad \beta^2=\mu/\varrho\,,\\ \lambda &= 2\mu\nu/(1-2\nu)\,. \end{aligned}$$

b_z is the slip produced along the slip surface defined by $y=0$, $x<0$ during the oscillations, μ and ν are the shear modulus and Poisson's ratio, respectively. Y_n and J_n are Bessel functions of first and second kind.

The contribution to the scattering cross section from the static displacement field has been already calculated and therefore only the contribution from the time-dependent displacement field remains to be evaluated.

The divergence, div $\mathbf{s}_\omega(t)$, of the time-dependent displacement field is given by

$$\begin{aligned}\operatorname{div}\mathbf{s}_\omega(t) = &-\frac{b_z K_\beta A}{8}\Big\{\Lambda^3\Big[\cos\Big(\tan^{-1}\frac{y}{x}\Big)\\ &\times\Big(\frac{y}{\{x^2+y^2\}^{1/2}}Z_0^\alpha-\frac{2y}{x^2+y^2}Z_1^\alpha\Big)\\ &+\cos 3\Big(\tan^{-1}\frac{y}{x}\Big)\frac{y}{\{x^2+y^2\}^{1/2}}Z_2^\alpha\Big]\\ &-\cos 3\Big(\tan^{-1}\frac{y}{x}\Big)\frac{y}{\{x^2+y^2\}^{1/2}}Z_2^\beta\\ &+\cos\Big(\tan^{-1}\frac{y}{x}\Big)\Big(\frac{y}{\{x^2+y^2\}^{1/2}}Z_0^\beta\\ &-\frac{2y}{x^2+y^2}Z_1^\beta\Big)\Big\}\\ &-\frac{b_z K_\beta A}{8}\Big\{\Lambda^3\Big[\sin\Big(\tan^{-1}\frac{y}{x}\Big)\\ &\times\Big(\frac{x}{\{x^2+y^2\}^{1/2}}Z_0^\alpha-\frac{2x}{x^2+y^2}Z_1^\alpha\Big)\\ &-\sin 3\Big(\tan^{-1}\frac{y}{x}\Big)\frac{x}{\{x^2+y^2\}^{1/2}}Z_2^\alpha\Big]\\ &+\sin 3\Big(\tan^{-1}\frac{y}{x}\Big)\frac{x}{\{x^2+y^2\}^{1/2}}Z_2^\beta\\ &+\sin\Big(\tan^{-1}\frac{y}{x}\Big)\Big(\frac{x}{\{x^2+y^2\}^{1/2}}Z_0^\beta\\ &-\frac{2x}{x^2+y^2}Z_1^\beta\Big)\Big\}. \qquad (35)\end{aligned}$$

The corresponding small-angle scattering cross section is then given by:

$$\frac{d\sigma}{d\Omega}=\frac{N}{V^2}a^2\left|\int_{-\infty}^{+\infty}dx\int_{-\infty}^{+\infty}dy\int_{-\infty}^{+\infty}\operatorname{div}\mathbf{s}_\omega(t)dz\right|^2. \qquad (36)$$

The influence of the frequency of oscillation on the total scattering cross section, which is the sum of the time-independent and the time-dependent scattering cross sections, is shown in Fig. 5.

The small-angle scattering cross section assumes an oscillatory behaviour which becomes more pronounced in amplitude for increasing values of the frequency of oscillation.

The oscillations in the curves of the scattering cross section *versus* the scattering vector take place approximately about the scattering curve corresponding to a zero-frequency or stationary dislocation. Oscillations from dislocations can thus easily be detected from small-angle scattering cross-section curves, which should exhibit an oscillatory behaviour around the scattering curve for a zero-frequency or stationary dislocation.

4. Scattering from dislocation loops and dislocation networks

4.1 *Stationary dislocation loops consisting of finite numbers of straight segments*

The results obtained for a straight dislocation of finite length can be used for all dislocation loops which consist of finite numbers of segments. For instance in a triangular dislocation loop, the stress field is the sum of contributions from these three segments.

We have calculated numerically the small-angle scattering cross section for several geometrical loops (triangle, rectangle, square, pentagon, hexagon, dodecagon), which, however, always have the same perimeter. The direction and the intensity of the Burgers vector for each segment of any geometrical figure are reported in Fig. 6.

It is interesting to point out (Fig. 6) that the peak in the scattering cross-section curve for a scattering vector parallel to the y direction is displaced toward higher values of the scattering vector on going from a triangular loop to a dodecagon loop. This is because all the closed loops of dislocations have been chosen with the same perimeter. In fact, it is known from variational theory that for a fixed perimeter, the circle presents the largest area among all the possible geometrical figures. In the present case the dodecagon presents the largest area among the geometrical figure that have been considered. So the larger the area, the

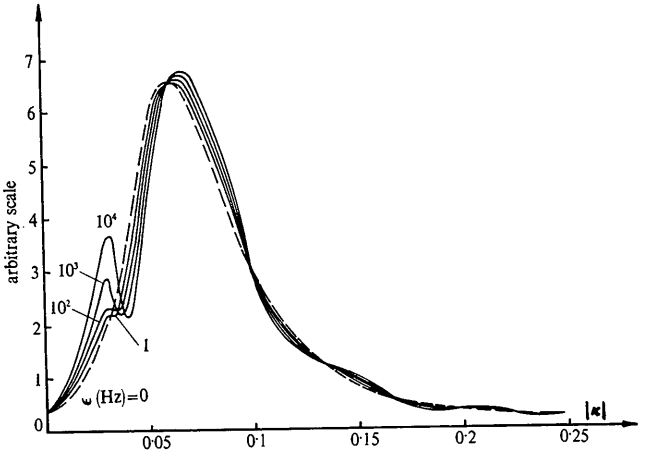

Fig. 5. Neutron small-angle scattering cross section as a function of the scattering amplitude $|\kappa|$ [κ perpendicular both to the slip direction (x axis) and to the dislocation line (z direction)] for different values of the oscillating frequency. For the parameters for the MBBA homogeneously oriented nematic liquid crystal see Fig. 2.

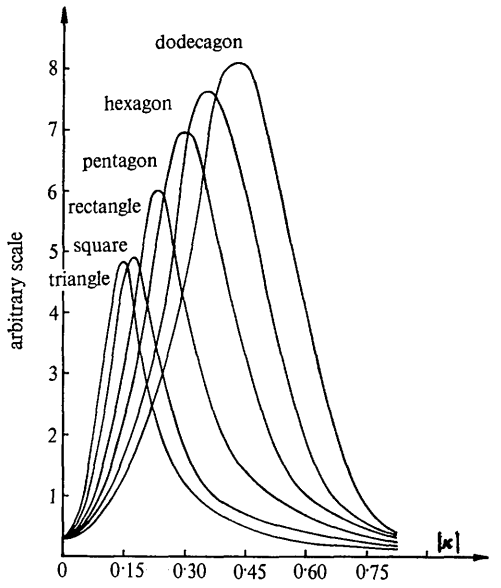

Fig. 6. Curves of the neutron small-angle scattering cross section *versus* the scattering vector in the y direction for several dislocation loops consisting of finite numbers of straight segments. The loops have the same perimeter which has been taken equal to 0·6 μm. For the parameters for the MBBA homogeneously oriented nematic liquid crystal see Fig. 2. The Burgers vector is perpendicular to each segment of any geometrical figure and has a constant intensity of 0·05 μm. All Burgers vectors point towards the inside of the loops.

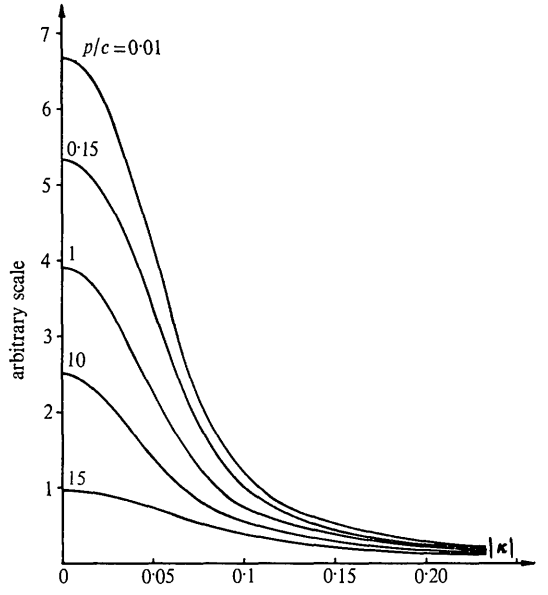

Fig. 7. Neutron small-angle scattering cross-section curves for helical dislocation with a constant radius c ($=0{\cdot}3$ μm) and a variable pitch p. (The scattering vector κ lies in a plane perpendicular to the axis of the helix). For the parameters for the MBBA homogeneously oriented nematic liquid crystal are Poisson ratio $\nu=0{\cdot}49$, shear modulus $\mu=10^{-5}$ Newton/m^2, $l=15$ μm.

smaller the value of the scattering vector for which the peak of the scattering curve occurs.

It is interesting to point out that the scattering curves for single straight dislocations are sharper than the corresponding ones for dislocation loops consisting of finite numbers of dislocation segments, as inspection of Fig. 2 and Fig. 6 shows at once. The peaks of the scattering curves for single straight dislocations occur at values of the scattering vector that are noticeably smaller than those for dislocation loops. This fact provides an easy means of discriminating between single dislocation segments and dislocation loops simply by comparison of the experimental scattering cross sections with the theoretical ones.

The scattering from a circular loop will be examined in the next section.

4.2 *Stationary curved dislocations*

In the continuum theory of dislocations it is well known that the equilibrium form of dislocation segments is a straight line, circle or helix. The possibility of the formation of a helical dislocation from a screw dislocation was first put forward by Seitz (1952) and the existence of such helical forms has been experimentally verified by many investigators since the initial observations by Bontinck & Amelinckx (1957).

The helical form is of great importance, since dislocation tangles in homogeneously oriented nematic liquid crystals may be interpreted on the basis of such dislocations. It is to be expected that helical dislocations have consistent characteristics for a pitch varying over a considerable range.

Expressions for the stress field of a helical dislocation of uniform shape with the Burgers vector along its axis have been obtained and solved numerically by Owen & Mura (1967*b*).

A study of the numerical results obtained for a helical dislocation of radius c and pitch p shows that the scattering decreases considerably when the pitch p becomes much larger than the radius c and the helix approximates a straight screw dislocation running in the z direction. In fact, as the pitch becomes infinite the stress field becomes that associated with a straight screw dislocation, which yields no small-angle scattering.

Moreover, for a long helix the degree of asymmetry with respect to any plane normal to the axis is small and the helix also exhibits almost axial symmetry with respect to its axis. For this reason the peak in the scattering curves of Fig. 7 appears at zero scattering vector, the scattering vector being in a plane normal to the axis of the helix.

For the same reasons, the equicontour lines for the scattered intensity as a function of the angle between the scattering vector and an arbitrary reference axis, both contained in a plane perpendicular to the axis of the helix, are concentric circles. In fact, Fig. 8 shows, for several values of the ratio between the pitch and the radius of the helix, equicontour lines for the rela-

tive scattered intensity, which are all circles centred on the origin, which also coincides with the relative scattered intensity curve of a screw dislocation.

At this point it should be interesting to examine the scattering curves for a circular dislocation loop. The analytic expressions for the stress field of a circular dislocation loop can be obtained from the general expressions for helical dislocation configurations in cylindrical coordinates, as given by Owen & Mura (1967*b*). The Burgers vector in this case everywhere lies tangential to the line element of the dislocation.

The actual calculation and the final expressions are somewhat lengthy and involved and, therefore, they will not be reproduced here. Only the normal component in the z direction of the stress field will be given because of its relative simplicity:

$$s_z = \frac{\mu b}{2\pi(1-\nu)}\left\{(r+c)^{-1}K\left(\frac{2(rc)^{1/2}}{r+c}\right) - (r-c)^{-1}E\left(\frac{2(rc)^{1/2}}{r+c}\right)\right\}, \qquad (37)$$

where $r=(x^2+y^2)^{1/2}$, c is the radius of the circular loop, E and K are the modified Bessel functions of zero order of the first and second kinds respectively. It can be shown that the remaining components of the stress field contain terms of a form similar to equation (37).

The corresponding scattering cross sections for a circular dislocation loop having Burgers vector everywhere tangential to the line element of the dislocation are shown in Fig. 9 for several values of the radius c.

As for the case of helical dislocations, the peak of the scattering curve is found for a zero scattering vector owing to the symmetry of the scattering configuration.

For increasing values of the radius, the intensity of the peak decreases and the scattering curve becomes flatter.

4.3 *Scattering from a plane dislocation network*

The most representative plane dislocation network is the Frank network, which has also been the most studied configuration in the past.

The Frank dislocation network forms a plane regular hexagonal system as shown in Fig. 10, situated a distance d from the interface coinciding with the xy plane.

The edge length of the regular hexagon is taken as $2a$. The whole network may be considered to be three systems of dislocation segments parallel to AB, CD and AF, denoted by the superscripts 1, 2 and 3, respectively. The density of dislocations parallel to AB (denoted by the superscript 1) has been expressed by Owen & Mura (1967*a*) as a combination of Fourier integrals and Fourier series. The density of dislocations parallel to BC can be expressed in a similar form by changing the coordinate system to ξ and η axes and taking the origin of coordinates at the midpoint of BC. A similar treatment can also be given for the dislocations parallel to FA by changing the coordinate system to ξ' and η' axes and taking the origin of coordinates at the midpoint of AF.

The total stress field due to all the dislocations is the sum of the three fields contributed by dislocations parallel to BC, CD and AF.

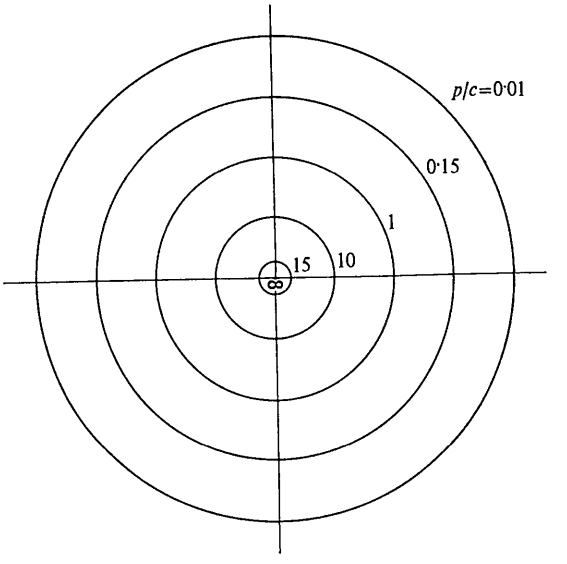

Fig. 8. Equicontour lines $|\tilde{\theta}|^2$ for the relative scattered neutron intensity as a function of the angle between the scattering vector κ and the y direction for several values of the ratio between the pitch and the radius of the helix. For the parameters for the MBBA homogeneously oriented nematic crystal see Fig. 7.

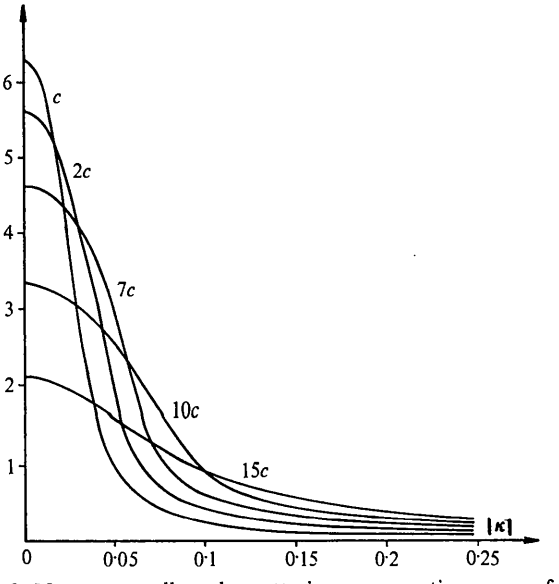

Fig. 9. Neutron small-angle scattering cross-section curves for circular dislocation loops having Burgers vector tangential to the line element of the dislocation everywhere for several values of the radius of the circular loop (the scattering vector lies in a plane perpendicular to the axis of the circle). For the parameters for the MBBA homogeneously oriented nematic liquid crystal see Fig. 7.

The actual calculation and the final expression are somewhat lengthy and cumbersome, and therefore, they will not be reproduced here in their entirety. Only the normal stress component of the total stress field will be given because of its relative simplicity and for background information only. Detailed calculations of the remaining stress components can be found in Owen & Mura (1967*a*). We have for the stress component in the z direction

$$\sigma_z = -\frac{2\mu(\lambda+\mu)}{\lambda+2\mu}\frac{1}{3a/3} \times \left\{ b_2^{(1)} \sum_{n=2,4\ldots} N(z+d)\exp\{iN(y+i|z+d|)\} \right.$$

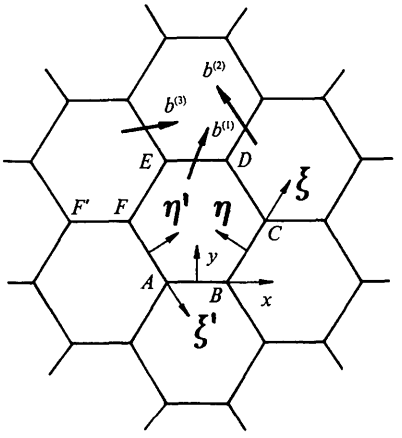

Fig. 10. Illustration of Frank network of dislocation indicating Burgers vectors and the three coordinate systems.

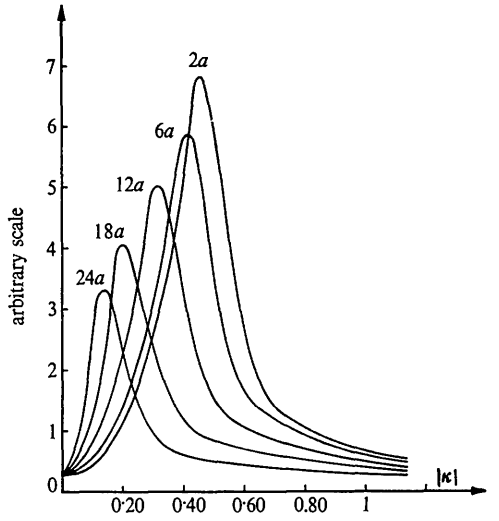

Fig. 11. Curves of the neutron small-angle scattering cross section *versus* the scattering vector taken parallel to the y axis for several values of the edge length, $2a$, of the hexagon. The parameters for the MBBA homogeneously oriented nematic liquid crystal are: Poisson ratio $\nu=0{\cdot}49$; shear modulus $\mu=10^{-5}$ Newton/m^2; $l=15$ μm; $a=0{\cdot}1$ μm.

$$+\sum_{m+n=2,4,\ldots}\frac{\sin aM}{aM}|z+d|\sqrt{(M^2+N^2)} \times\exp\{-|z+d|\sqrt{(M^2+N^2)}\} \times\{(MNb_1^{(1)}/b_2^{(1)}+N^2)\exp\{i(Mx+Ny)\} +(-MNb_1^{(1)}/b_2^{(1)}+N^2)\exp\{i(Mx-Ny)\}$$

$$+b_2^{(2)}\sum_{n=2,4,\ldots}N(z+d)\exp\{iN(\eta+i|z+d|\} +\sum_{m+n=2,4,\ldots}\frac{\sin aM}{aM}|z+d|\sqrt{(M^2+N^2)} \times\exp\{-|z+d|\sqrt{(M^2+N^2)}\} \times\{(MNb_1^{(2)}/b_2^{(2)}+N^2)\exp\{i(M\xi+N\eta)\} +(-MNb_1^{(2)}/b_2^{(2)}+N^2)\exp\{i(M\xi-N\eta)\}$$

$$+b_2^{(3)}\sum_{n=2,4,\ldots}N(z+d)\exp\{iN(\eta'+i|z+d|\} +\sum_{m+n=2,4,\ldots}\frac{\sin aM}{aM}|z+d|\sqrt{(M^2+N^2)} \times\exp\{-|z+d|\sqrt{(M^2+N^2)}\} \times(MNb_1^{(3)}/b_2^{(3)}+N^2)\exp\{i(M\xi'+N\eta')\} +(-MNb_1^{(3)}/b_2^{(3)}+N^2)\exp\{i(M\xi'-N\eta')\}\Big\}$$

with

$$M=m\pi/3a \quad \text{and} \quad N=n\pi(a/3)\,. \tag{38}$$

The remaining components of the stress field of the dislocation network contain terms of a form similar to equation (38), as shown by Owen & Mura (1967*a*).

The divergence of the displacement field can be calculated by using equations (4)–(5). Then the small-angle scattering cross section of a Frank dislocation network can be evaluated by numerical integration, through the use of equations (1) and (2).

The general characteristic of the stress field components is that the stress field is inversely proportional to the edge length of the hexagon, $2a$, and decreases exponentially with the distance from the plane of the network.

For example, the values of σ_z along the z axis at $x=0$, $y=a/3$ (intersecting the centre of the hexagon) reach a maximum value at about $z=a$, and the components $b_1^{(i)}$, namely the screw components, do not contribute to the normal stress. The stress magnitude depends only on the term $(b_2^{(1)}+b_2^{(2)}+b_2^{(3)})$, which must equal $3b_2^{(1)}$ from the law of conservation of Burgers vector at a node, namely $b_2^{(1)}=(b_2^{(2)}+b_2^{(3)})\cos 60°$.

The effect of the edge length, $2a$, of the regular hexagon forming a plane regular hexagonal dislocation network, on the shape of the small-angle scattering cross section is reported in Fig. 11. The scattering vector has been taken parallel to the y axis. For increasing edge lengths, the peak in the scattering cross-section curves is shifted toward smaller values of the scattering vector and decreases in intensity. It is therefore possible to draw the peak value of the scattered intensity as a function of the edge length $2a$ of the regular hexagon.

For increasing values of the edge length there is a very noticeable decrease of the scattered intensity, as Fig. 12 shows very clearly.

5. Conclusion

The existence of lines or regions of discontinuity in the ordered structure of homogeneously oriented nematic liquid-crystal layers makes possible the setting up of dislocations of various kinds. We have shown that the shape of the small-angle scattering curves is mainly determined by the kind of dislocation configuration exhibited by homogeneously oriented nematic liquid crystals. As a consequence we have made a complete examination of the shape of the neutron scattering curves at very small scattering vectors, of the order of $0{\cdot}05 \sim 0{\cdot}1$ nm^{-1}, for the most significant cases of dislocation configurations.

This study gives a partial guide to the construction and the interpretation of scattering relations for any kind of possible dislocation configuration in homogeneously oriented nematic liquid crystals, *e.g.* for stationary straight edge dislocations, moving edge dislocations, oscillating edge dislocations, curved dislocations and dislocation networks.

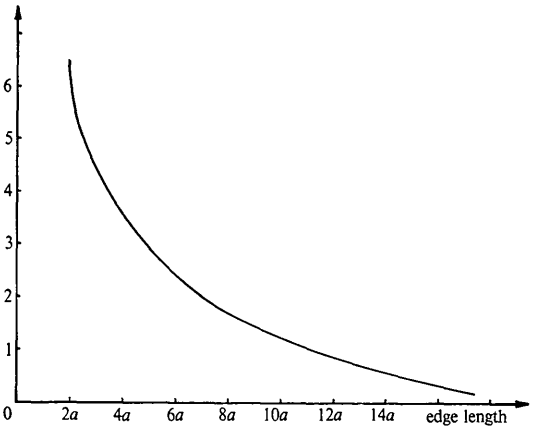

Fig. 12. Behaviour of the peak value of the scattered intensity *versus* the edge length $2a$ of the regular hexagon of a plane regular hexagonal Frank dislocation network (The scattering vector has been taken parallel to the y axis). For the parameters for the MBBA homogeneously oriented nematic liquid crystal see Fig. 11.

References

BONTINCK, W. & AMELINCKX, S. (1957). *Phil. Mag.* **2**, 94–101.

BURGERS, J. M. (1939). *Koninkl. Ned. Akad. Wetenschap. Proc.* **42**, 293–314.

ESHELBY, J. D. (1949*a*). *Proc. Roy. Soc.* A**61**, 396–401.

ESHELBY, J. D. (1949*b*). *Proc. Roy. Soc.* A**62**, 307–396.

ESHELBY, J. D., READ, W. T. & SHOCKLEY, W. (1953). *Acta Met.* **1**, 251–264.

FRANK, F. C. (1949). *Proc. Phys. Soc.* A**62**, 131–158.

KIUSALAAS, J. & MURA, T. (1964). *Phil. Mag.* **9**, 1–16.

KRIVOGLAZ, M. A. (1969). *Theory of X-ray and Thermal Neutron Scattering by Real Crystals*. New York: Plenum Press.

LEIBFRIED, G. (1953). *Z. Phys.* **135**, 23–49.

LOVE, A. E. H. (1944). *The Mathematical Theory of Elasticity*. New York: Dover.

OLIVEI, A. (1973). *Acta Cryst.* A**29**, 692–701.

OWEN, D. R. J. & MURA, T. (1967*a*). *J. Appl. Phys.* **38**, 1999–2009.

OWEN, D. R. J. & MURA, T. (1967*b*). *J. Appl. Phys.* **38**, 2818–2835.

SCHMATZ, W. (1975). *Riv. Nuovo Cim.* **5**, 398–422.

SEITZ, F. (1952). *Advanc. Phys.* **1**, 43–74.

Acta Cryst. (1976). A**32**, 994

Statistical Bias in Least-Squares Refinement

BY A. J. C. WILSON

Department of Physics, University of Birmingham, Birmingham B15 2TT, England

(*Received* 20 *February* 1976; *accepted* 14 *May* 1976)

Statistical fluctuations in counting rates *etc.*, as well as defects in the structural model, can introduce bias in the estimation of parameters by least-squares refinements. Of the residuals in common use, only unweighted $R_2 = \sum(I_o - I_c)^2$ is free from statistical bias. Order-of-magnitude estimates of the bias can be derived, but it seems better to avoid it by adjusting the weights. To the second order, refinement of R_2 is unbiased if the intensity used in calculating the usual weights is not I_o but $\frac{1}{3}(I_o + 2I_c)$. There seems to be no simple method of avoiding bias in R_1.

Introduction

Estimates of quantities obtained by or from physical measurements may differ from the true values for one or more of three reasons.

(i) Systematic errors (defects in the model). In crystallographic investigations these may include incorrect allowance for absorption or extinction, incorrect assumptions about atomic scattering factors or thermal motion, overloading of counters or amplifiers, and so on (Shoemaker, 1968; Wilson, 1973).

(ii) Random errors. In crystallographic investiga-